Journal of Ovarian Research

RESEARCH

Open Access

Pan-cancer profiling links *C1orf50* to DNA repair and immune modulation in ovarian cancer

Anna Rogachevskaya[1,2†], Yusuke Otani[1,2,6†], Akira Ohtsu[2,3,4], Vanessa D. Chin[5], Tirso Peña[1,2], Seiji Arai[4], Shinichi Toyooka[6], Atsushi Fujimura[7*] and Atsushi Tanaka[1,2,8*]

Abstract

Background *C1orf50* encodes a small, evolutionarily conserved protein, the function of which remains unclear. Its significance across various human cancers, particularly its specific role in ovarian cancer within an immunogenomic context, is not yet fully understood. Utilizing The Cancer Genome Atlas and single-cell RNA sequencing (scRNA-seq) public datasets, we conducted a comprehensive profiling of *C1orf50* across multiple cancer types, with a particular focus on ovarian cancer, to investigate its associations with copy-number status, genomic instability, tumor programs, and the immune microenvironment.

Results Across cancer types, copy-number gain or amplification of *C1orf50* was most frequent in ovarian cancer and closely tracked with higher messenger RNA levels. Higher *C1orf50* expression was associated with a greater tumor mutational burden and homologous recombination deficiency, as indicated by gene-set patterns that suggested heightened cell-cycle and cellular stress responses accompanied by reduced oxidative phosphorylation, enrichment of regulatory T cells, and depletion of resting memory CD4 T cells. In ovarian cancer, focal events at chromosome 1p34.2 were accompanied by stepwise increases in *C1orf50* expression by clinical stage and were linked to higher tumor mutational burden, homologous recombination deficiency, and greater loss of heterozygosity, together with more frequent gene alterations in *BRCA1* or *BRCA2*. Immune composition clustered into profiles consistent with an immunosuppressive context in tumors with higher *C1orf50* expression. The scRNA-seq data further revealed that cancer cells enhanced immune-suppressive interactions with various immune cell populations and diminished antigen-presentation signals. Analyses of genomic instability in ovarian cancer suggested mutational processes compatible with base-substitution patterns associated with cytidine deaminase activity and with insertion-deletion patterns characteristic of homologous recombination failure, while transcript-level patterns pointed to a broad

†Anna Rogachevskaya and Yusuke Otani contributed equally to this work.

*Correspondence:
Atsushi Fujimura
fujimura.atsushi@kagawa-u.ac.jp
Atsushi Tanaka
atanaka@bidmc.harvard.edu

Full list of author information is available at the end of the article

downshift of canonical DNA repair activity with apparent compensatory adjustments in related pathways rather than a uniform change in any single pathway.

Conclusions The overexpression of *C1orf50* characterizes an aggressive immunogenomic phenotype in ovarian cancer, distinguished by genomic instability, impaired DNA repair mechanisms, and extensive immunosuppression. These findings indicate that *C1orf50* warrants consideration as a potential biomarker and a prospective target for therapeutic investigation. Furthermore, they advocate for the progression to prospective validation and functional studies to ascertain its clinical significance.

Keywords *C1orf50*, Pan-cancer analysis, DNA repair, Gene expression, Tumor microenvironment, Immune evasion, Single-cell RNA-seq

Introduction

C1orf50 (Chromosome 1 open reading frame 50) is a gene located on chromosome 1p34.2 that encodes a small protein of ~ 26 kDa (DUF2452). *C1orf50* is a highly conserved gene, with homologs present across a wide range of species, from *Caenorhabditis elegans* to mammals. This level of conservation usually indicates an essential biological function that has been preserved through evolution. However, despite this, the molecular functions of *C1orf50* remain largely unknown, and the gene is still considered poorly characterized. Structural predictions from AlphaFold [1] provide initial clues, suggesting the protein folds into a compact, hairpin-like structure composed of two α-helices. Such a minimal fold suggests that *C1orf50* may function as a small structural or regulatory protein rather than a typical enzyme. Transcriptomic analyses also reveal two annotated isoforms: one protein-coding and the other non-coding, indicating that *C1orf50* may operate at multiple regulatory levels. Overall, these findings identify *C1orf50* as an intriguing yet underexplored gene that likely plays an important role in cellular biology and merits deeper functional investigation.

We have previously identified *C1orf50* as a prognostic biomarker in malignant melanoma [2], hepatocellular carcinoma [3], and Luminal A breast cancer [4]. In melanoma, high levels of *C1orf50* are associated with poor clinical outcomes, as the gene appears to promote tumor progression by accelerating cell cycle activity, enhancing DNA damage repair, and supporting cancer stemness through YAP/TAZ signaling [2]. A similar trend is seen in Luminal A breast cancer, where increased *C1orf50* expression is linked to a worse prognosis, aiding tumor cell proliferation, maintaining stem-like features, and increasing resistance to therapy. Besides its role in tumor growth, *C1orf50* also influences immune-related transcriptional programs, including the upregulation of *PD-L1*, which helps tumors evade immune surveillance [4]. Importantly, these molecular and functional features have also been confirmed experimentally in our previous wet-lab studies. Using immunohistochemistry and Western blotting with a specific anti-C1orf50 antibody (Proteintech #20,957–1-AP, raised against the 1–199 aa domain of human C1orf50 [BC001711]), we validated that C1orf50 protein expression correlates with enhanced cell-cycle activity and cancer stemness in breast cancer, with stemness-related phenotypes in melanoma, and with stem-like features in hepatocellular carcinoma. These findings demonstrate that the oncogenic and stemness-promoting functions of C1orf50 are consistently supported by both transcriptomic analyses and direct experimental evidence.

These observations support a role for *C1orf50* as an oncogenic factor that integrates tumor cell-intrinsic programs with modulation of the tumor immune microenvironment. However, its broader biological and clinical relevance across diverse human cancers has not been systematically evaluated.

Genomic profiling has identified recurrent copy number gains and focal amplifications at 1p34.2, which include C1orf50, across various malignancies, such as ovarian cancer, neuroblastoma, and lung adenocarcinoma [5–7]. Genomic instability is a hallmark of cancer, accelerating tumor evolution, driving therapy resistance, and predicting poor outcomes [8, 9]. By increasing tumor mutation burden and generating neoantigens, it can also reshape the immune landscape and influence responsiveness to immune checkpoint blockade [10]. *C1orf50* may contribute to this process by supporting proliferative and DNA repair programs while simultaneously modulating immune pathways such as *PD-L1* expression, linking genomic instability to both tumor progression and immune escape.

Based on our prior observations linking *C1orf50* to cell-cycle regulation, stemness, and immune modulation, we hypothesized that *C1orf50* functions at the intersection of genomic instability and immune regulation, driving cancer progression through dual effects on tumor biology and the tumor microenvironment. To investigate this hypothesis, we conducted a comprehensive pan-cancer analysis of The Cancer Genome Atlas (TCGA) to characterize *C1orf50* expression, mutation spectrum, and copy number alterations across 33 cancer types, and to evaluate their associations with genomic instability metrics and immune cell infiltration. Given that *C1orf50*

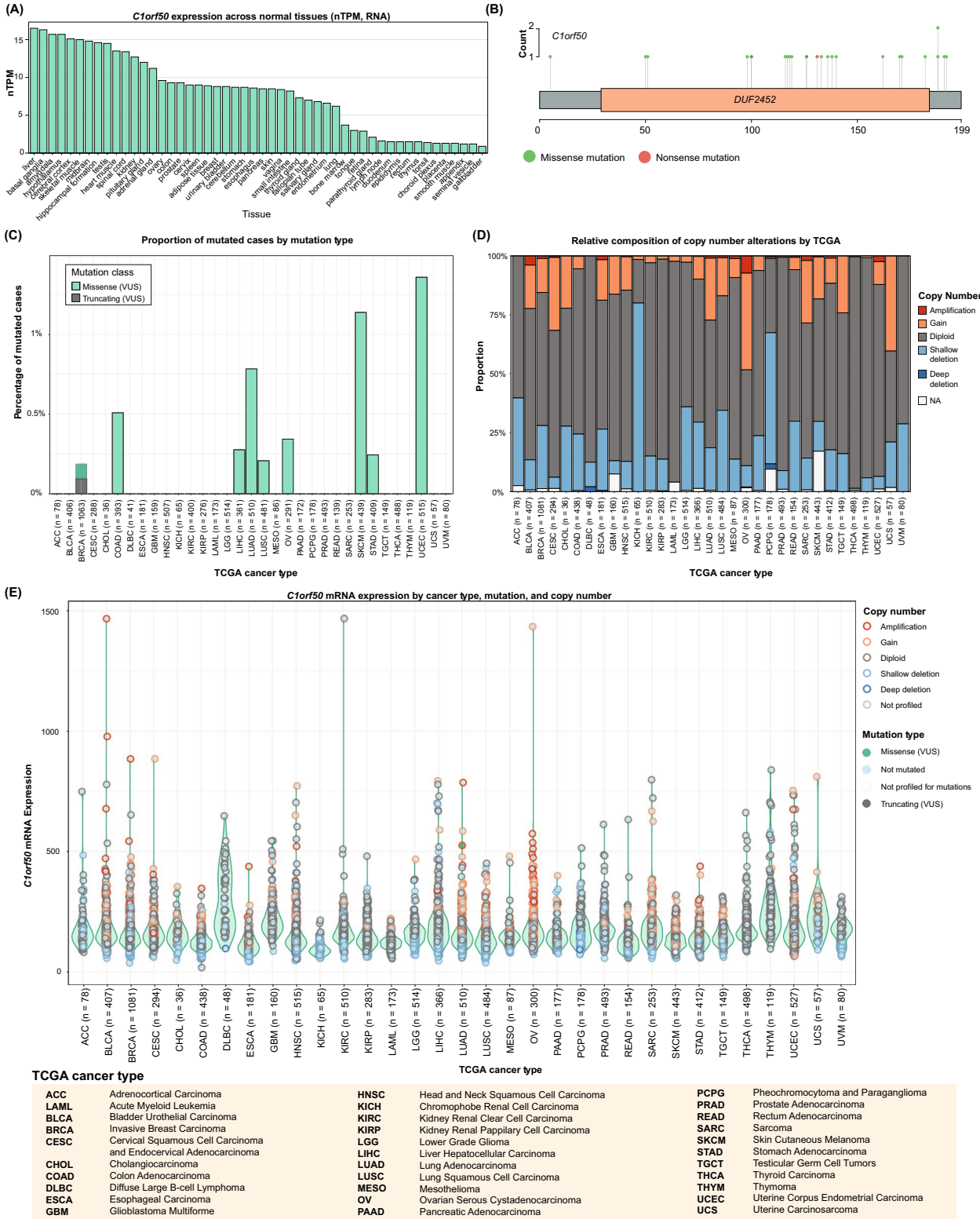

ACC	Adrenocortical Carcinoma	**HNSC**	Head and Neck Squamous Cell Carcinoma	**PCPG**	Pheochromocytoma and Paraganglioma
LAML	Acute Myeloid Leukemia	**KICH**	Chromophobe Renal Cell Carcinoma	**PRAD**	Prostate Adenocarcinoma
BLCA	Bladder Urothelial Carcinoma	**KIRC**	Kidney Renal Clear Cell Carcinoma	**READ**	Rectum Adenocarcinoma
BRCA	Invasive Breast Carcinoma	**KIRP**	Kidney Renal Papillary Cell Carcinoma	**SARC**	Sarcoma
CESC	Cervical Squamous Cell Carcinoma and Endocervical Adenocarcinoma	**LGG**	Lower Grade Glioma	**SKCM**	Skin Cutaneous Melanoma
		LIHC	Liver Hepatocellular Carcinoma	**STAD**	Stomach Adenocarcinoma
CHOL	Cholangiocarcinoma	**LUAD**	Lung Adenocarcinoma	**TGCT**	Testicular Germ Cell Tumors
COAD	Colon Adenocarcinoma	**LUSC**	Lung Squamous Cell Carcinoma	**THCA**	Thyroid Carcinoma
DLBC	Diffuse Large B-cell Lymphoma	**MESO**	Mesothelioma	**THYM**	Thymoma
ESCA	Esophageal Carcinoma	**OV**	Ovarian Serous Cystadenocarcinoma	**UCEC**	Uterine Corpus Endometrial Carcinoma
GBM	Glioblastoma Multiforme	**PAAD**	Pancreatic Adenocarcinoma	**UCS**	Uterine Carcinosarcoma

Fig. 1 (See legend on next page.)

(See figure on previous page.)

Fig. 1 Genomic alterations and mRNA expression of *C1orf50* across 33 TCGA cancer types. **A***C1orf50* mRNA expression levels (nTPM) in normal human tissues based on the Human Protein Atlas Consensus dataset. **B** Lollipop plot showing the distribution of somatic mutations in *C1orf50* (transcript variant 1, NM_024097) across TCGA pan-cancer samples. Green dots represent missense mutations, and red dots represent nonsense mutations. The vertical axis indicates the number of samples harboring a mutation at the same amino acid position. **C** Proportion of mutated cases by mutation type across 33 TCGA cancer types. Missense (VUS) and truncating (VUS) mutations are shown separately. **D** Relative composition of copy-number alteration categories (amplification, gain, diploid, shallow deletion, deep deletion) in *C1orf50* across TCGA cancer types. **E** Violin plots showing *C1orf50* mRNA expression levels by cancer type, mutation status, and copy-number category. Circles represent individual tumor samples; colors indicate mutation type and copy-number status as defined in the legend

amplification occurs most prominently in ovarian cancer, we concentrated our analysis on this setting. Through integration of transcriptomic, proteomic, and single-cell communication data, we identified the molecular pathways influenced by *C1orf50,* and we evaluated its potential clinical significance as both a biomarker and a therapeutic target.

Methods

Data sources and preprocessing

All analyses were conducted using R (v4.3.2; University of Auckland, Auckland, New Zealand) [11]. Genomic, transcriptomic, proteomic, and normal tissue expression data were obtained from The Cancer Genome Atlas (TCGA) and other publicly available resources. The TCGA Pan-Cancer dataset, accessed through the cBioPortal for Cancer Genomics [12, 13] provided four key metrics of genomic instability: the chromosomal instability (CIN) index, the fraction of genome altered (FGA), the microsatellite instability (MSI) sensor score, and the tumor mutation burden (TMB). Homologous recombination deficiency (HRD) scores and CIBERSORT-derived estimates of immune cell infiltration were obtained from the dataset of Thorsson et al. [14], and loss of heterozygosity (LOH) data were obtained from the dataset of Taylor et al. [15]. CIBERSORT data were available for 32 TCGA cancer types, excluding the acute myeloid leukemia (LAML) cohort, which lacked valid fraction values. All metrics were matched to the corresponding TCGA sample identifiers for downstream analyses. For the pan-cancer analysis, we utilized the "Batch normalized from Illumina HiSeq_RNASeqV2" mRNA expression dataset from the TCGA Pan-Cancer Atlas, accessed via cBioPortal. These data were generated using RSEM [16] for gene-level normalization to correct for sequencing depth and transcript length, followed by EB+ +(a ComBat-based empirical Bayes harmonization method) [17] to adjust batch effects arising from different Illumina platforms, sequencing centers, and experimental plates. From this harmonized dataset available through cBioPortal, we obtained C1orf50 expression values across all tumor types, ensuring direct comparability of expression measurements throughout the TCGA cohort. For the cancer type-specific analyses, we used mRNA expression z-scores from cBioPortal. Samples were stratified into *C1orf50*-high and *C1orf50*-low groups based on the median expression level, using the maximum number of available samples for each analysis. In the ovarian cancer cohort, 300 cases with both RNA expression and copy-number alteration (CNA) data were used in this study. Among these, the most extensive available datasets with matched mutation data ($n = 291$) and clinical FIGO stage information ($n = 296$) were used for the respective analyses. Each analysis used all available samples for that data type, without arbitrary exclusions, to ensure transparency and reproducibility.

Single-cell RNA sequencing data preprocessing and annotation

Single-cell RNA sequencing (scRNA-seq) data were obtained from a publicly available dataset (GSE158722), which includes 10 × Genomics profiles from 20 ovarian tumor samples. We included both pre-treatment samples and post-treatment samples to maximize statistical power. Raw gene-cell count matrices were downloaded and processed with the Seurat package (v5.2.1) [18]. Each tumor sample was initially imported as a separate Seurat object before merging for integrated analysis. To maintain data quality, we applied strict quality control, excluding cells with fewer than 200 genes, more than 5,000 genes, or over 10% mitochondrial gene transcripts, as these often indicate stressed or dying cells. For gene-level filtering, a gene was considered expressed if it had non-zero counts in ≥ 3 cells across the merged object (Seurat default). We then normalized counts in Seurat using log-normalization (scale factor = 10,000), identified highly variable genes with the 'vst' method (2,000 features), followed by scaling and PCA for downstream analyses. Batch effects were corrected with Harmony (v1.2.3) [19] using sample ID as the batch variable. We used sample ID as the Harmony batch variable because libraries were generated at the sample level, which introduces technical variation across patients. We verified that integration improved sample mixing within cell types, supporting that batch effects were reduced without over-correction (Supplemental Fig. 1). The resulting batch-corrected embeddings were used for unsupervised clustering and visualization via Uniform Manifold Approximation and Projection (UMAP). Clustering employed the top 30 Harmony-corrected PCs, with a moderate resolution to capture both broad cell types and finer subpopulations. Initial cell type annotations were assigned based on the

GSE158722 annotation file. To refine immune cell classification, macrophages and CD4⁺ T cells were further subtyped. Macrophages were classified into M1-like (pro-inflammatory) or M2-like (anti-inflammatory) phenotypes based on gene expression scores derived from established marker sets. M1-like macrophages were characterized by high expression of *NOS2*, *IL1B*, *TNF*, *IL6*, and *IL12B*, while M2-like macrophages were characterized by high expression of *MRC1*, *CD163*, *TGFB1*, *IL10*, and *ARG1*. Cells with indeterminate scores were labeled as "Intermediate" and excluded from downstream analysis. Regulatory T cells (Tregs) within the CD4⁺ T cell population were identified by high expression of *FOXP3*, *IL2RA*, and *CTLA4*. We focused on key immune and tumor cell types, including B cells, CD4⁺ and CD8⁺ T cells, Tregs, NK cells, dendritic cells, monocytes, M1 and M2 macrophages, and malignant epithelial cells. The final dataset comprised 24,267 cells. This annotated and batch-corrected dataset was employed for all subsequent analyses.

Differential expression and genomic signature analysis

Differential expression analysis was performed using the limma package (v3.58.1). Mutational signatures were calculated using COSMIC Mutational Signatures v3.4. Protein expression profiles were obtained from the RPPA500 dataset downloaded from the TCPA portal (https://tcpaportal.org/rppa500/download.html) [20, 21]. Normal tissue RNA expression values (nTPM) were obtained from the consensus dataset of the Human Protein Atlas [22].

Gene set enrichment analysis (GSEA)

GSEA was performed in pre-ranked mode using fgsea (v1.28.0), ranking genes by limma moderated t-statistics for the *C1orf50*-high versus *C1orf50*-low comparison within each cancer type. The analyses were based on gene expression z-score data from the TCGA Pan-Cancer Atlas obtained via cBioPortal. MSigDB Hallmark (v2023.2.Hs) gene sets were used as the reference, and pathways with a false discovery rate (FDR-adjusted p value) < 0.05 were considered significant.

Copy-number analysis using GISTIC2.0

Segmented copy-number data for the TCGA ovarian cancer cohort were analyzed using GISTIC2.0 (v2.0.23) with Human_hg19.mat as the reference. Key parameters were set as follows: amplification/deletion thresholds = ± 0.1, focal length cutoff = 0.70, confidence level = 0.90, q-value cutoff = 0.01, and join segment size = 4. Both gene-level and broad-level analyses were enabled ("gene GISTIC" = yes; "run broad analysis" = yes) using "wide peak" boundaries. Segments were median-centered, capped at ± 2.0, and the X chromosome was retained. Gene-level CNA values were integrated with mRNA expression using matched TCGA sample IDs.

Unsupervised clustering of tumor immune profiles

CIBERSORT-derived immune cell fractions were initially pre-processed to ensure data quality. Samples with missing values were removed, and the remaining fractions were standardized using z-score transformation across all cell types to facilitate direct comparison. To identify patterns of immune composition, we used unsupervised k-means clustering with k = 3, which divided tumors into three distinct immune subtypes. These clusters, labeled C1 through C3, displayed consistent differences in immune cell infiltration profiles, providing a basis for further analysis of tumor-immune interactions. To evaluate the robustness of this clustering solution, we conducted a bootstrap stability analysis using 80% subsampling, repeated 1000 times. Agreement between subsampled clusters and the full dataset was quantified using both the Adjusted Rand Index (ARI) and Normalized Mutual Information (NMI). The results demonstrated strong reproducibility of the three-cluster solution (median ARI = 0.889, interquartile range 0.757–0.941; median NMI = 0.832, interquartile range 0.700–0.906).

Data visualization

Heatmaps were generated using the ComplexHeatmap package (v2.18.0) [23] for GSEA results and other comparative analyses. Statistical significance was indicated by asterisks where applicable.

Cell–cell communication analysis based on *C1orf50* expression

To examine the impact of variation in tumor-intrinsic *C1orf50* expression on intercellular communication, we conducted a comparative CellChat [24] analysis between malignant epithelial cells with high and low *C1orf50* expression. This analysis utilized a previously annotated and batch-corrected Seurat object comprising 20 tumor samples (GSE158722), which included major immune and tumor cell types as previously described. Malignant epithelial cells were divided into *C1orf50*-high and *C1orf50*-low groups based on the median expression level of *C1orf50*. All non-epithelial cell populations were included in both groups to allow a direct comparison of outgoing signaling from tumor cells to the surrounding immune microenvironment. Two distinct CellChat objects were constructed, one for each group, employing the human ligand-receptor database. Overexpressed genes and interactions were identified, and cell–cell communication probabilities were calculated. Interactions with low abundance were filtered by requiring a minimum of 10 cells per cell type. Communication probabilities were subsequently aggregated at the signaling

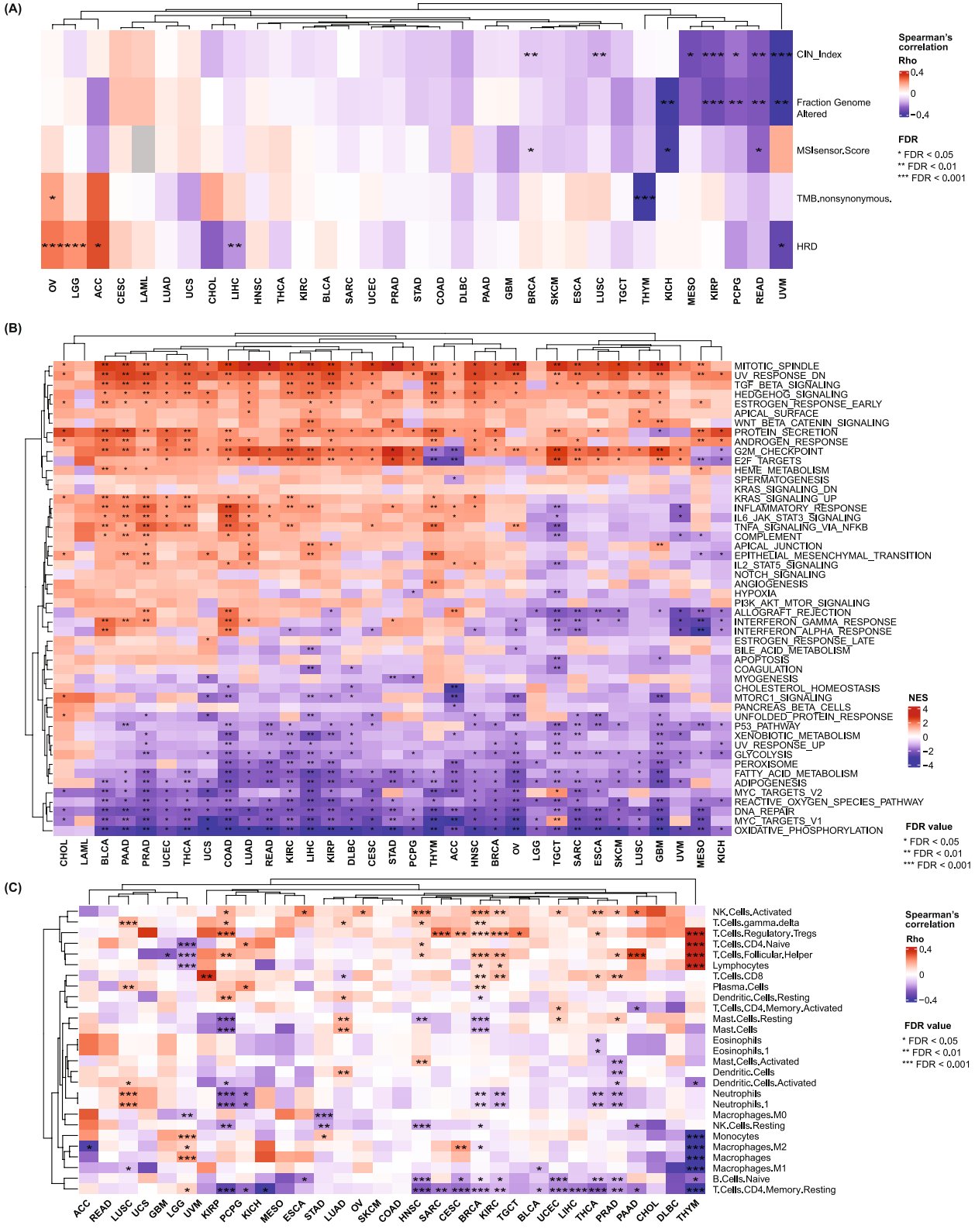

Fig. 2 (See legend on next page.)

(See figure on previous page.)

Fig. 2 Association of *C1orf50* expression with genomic instability, pathway activity, and immune cell composition across TCGA cancers. **A** Spearman correlations between *C1orf50* mRNA expression and key genomic instability metrics, including chromosomal instability (CIN) index, fraction of genome altered (FGA), microsatellite instability (MSI) score, tumor mutational burden (TMB), and homologous recombination deficiency (HRD) scores. Color scale denotes correlation coefficient (rho). Asterisks indicate statistical significance (* FDR < 0.05, ** FDR < 0.01, *** FDR < 0.001; false discovery rate adjusted using the Benjamini–Hochberg method). **B** Heatmap of normalized enrichment scores (NES) from Gene Set Enrichment Analysis (GSEA) using Hallmark gene sets, comparing *C1orf50*-high versus *C1orf50*-low tumors (median split) within each of the 33 TCGA cancer types. Significance is based on Benjamini–Hochberg adjusted FDR values (* FDR < 0.05, ** FDR < 0.01, *** FDR < 0.001). **C** Spearman correlations between *C1orf50* expression and CIBERSORT-estimated immune cell fractions across TCGA cancer types. Positive values indicate higher abundance, and negative values indicate lower abundance of the corresponding immune cell type in *C1orf50*-high tumors. Significance is based on Benjamini–Hochberg adjusted FDR values (* FDR < 0.05, ** FDR < 0.01, *** FDR < 0.001)

pathway level, and centrality scores were computed for each group. To evaluate the copy number differential communication between the two groups, the two CellChat objects were merged and compared. Interaction counts and total communication strength were summarized across cell types. Specifically, outgoing signaling from malignant epithelial cells to immune cells was analyzed to assess changes in potential immune-regulatory interactions associated with *C1orf50* expression.

Results

Genomic alterations and mRNA expression of *C1orf50* across 33 human cancer types

Normal tissue analysis of the Human Protein Atlas Consensus dataset showed that *C1orf50* RNA expression is highest in the liver, nervous system, testis, kidney, and ovary, while it is comparatively low in tissues such as the tonsil and gallbladder (Fig. 1A). Examination of somatic mutations in TCGA pan-cancer cohorts revealed that, within the 199 amino acids encoded by transcript variant 1 (NM_024097), missense mutations (green) were the most common. In contrast, nonsense mutations (red) were infrequent and scattered, with no evidence of recurrent hotspots (Fig. 1B). Mutation rates were generally low across all tumor types, reaching their highest levels in uterine corpus endometrial carcinoma (UCEC, 1.36%) and skin cutaneous melanoma (SKCM, 1.14%) (Fig. 1C).

Copy-number analysis identified frequent gains or amplifications in ovarian cancer (OV, 48.3%), uterine carcinosarcoma (UCS, 40.4%), and cervical squamous cell carcinoma and endocervical adenocarcinoma (CESC, 31.6%). In contrast, shallow or deep deletions were most common in pheochromocytoma and paraganglioma (PCPG, 57.9%) and chromophobe renal cell carcinoma (KICH, 80.0%) (Fig. 1D). When copy-number data were integrated with transcriptomic profiles, tumors with *C1orf50* amplification or gain—most notably ovarian cancers—consistently exhibited elevated mRNA expression (Fig. 1E). These findings indicate that copy-number amplification may play a key role in *C1orf50* overexpression in certain malignancies.

Association of *C1orf50* expression with genomic instability, pathway activity, and immune microenvironment in pan-cancer analysis

We then examined the relationship between *C1orf50* expression and various measures of genomic instability across 33 TCGA cancer types (Fig. 2A). Using Spearman correlation analysis, we found strong positive relationships in OV and adrenocortical carcinoma (ACC), where higher *C1orf50* levels correlated with increased tumor mutational burden (TMB) and homologous recombination deficiency (HRD) scores. These results suggest that C1orf50 may be associated with genomic instability in specific tumor types, potentially contributing to the accumulation of mutations and faulty DNA repair. Conversely, several cancers, including mesothelioma (MESO), pheochromocytoma and paraganglioma (PCPG), and rectum adenocarcinoma (READ), showed notable negative correlations, especially with chromosomal instability (CIN) and the fraction of genome altered (FGA). This suggests that the relationship between C1orf50 and genomic instability is inconsistent, varying by cancer type. Such variation highlights the possibility that C1orf50 may have context-dependent roles in genome maintenance, promoting or reducing instability depending on the cellular and molecular environment.

To identify associated biological programs, we performed GSEA by comparing *C1orf50*-high and *C1orf50*-low tumors, defined by the median expression within each cancer type (Fig. 2B). Consistent with prior observations [2–4], gene sets related to the mitotic spindle and downregulated genes in response to ultraviolet (UV) radiation were significantly enriched in the high-expression group across most cancers. In contrast, oxidative phosphorylation-related genes were broadly downregulated. These trends suggest that *C1orf50* overexpression is linked to proliferative and stress-response pathways, alongside suppression of mitochondrial oxidative metabolism.

Analysis of CIBERSORT-derived immune cell fractions showed that *C1orf50*-high tumors were significantly enriched in regulatory T cells (Tregs) across multiple cancer types, including thymoma (THYM), testicular germ cell tumors (TGCT), thyroid carcinoma (THCA), kidney renal clear cell carcinoma (KIRC), breast carcinoma

(BRCA), cervical squamous cell carcinoma and endocervical adenocarcinoma (CESC), sarcoma (SARC), and kidney renal papillary carcinoma (KIRP) (Fig. 2C). These findings suggest that *C1orf50* overexpression contributes to creating an immunosuppressive tumor microenvironment. Conversely, resting memory $CD4^+$ T cells were depleted in numerous cancer types, including THYM, KIRP, chromophobe renal cell carcinoma (KICH), and others potentially reflecting a shift toward activated or exhausted states. Collectively, these results indicate that *C1orf50* overexpression is associated with genomic instability in selected cancers, activation of cell cycle and stress pathways, and an immune landscape characterized by elevated regulatory T cell levels and reduced memory $CD4^+$ T cells, features consistent with immune evasion.

C1orf50 amplification leads to increased mRNA levels and immune evasion signatures in ovarian cancer

We next turned our analysis to ovarian cancer, where *C1orf50* showed frequent copy number gains and amplifications. Using GISTIC2.0 on the TCGA ovarian cancer cohort, we identified recurrent amplification at chromosome 1p34.2, the locus containing *C1orf50* (Fig. 3A). Tumors with copy-number gain or high-level amplification exhibited significantly higher *C1orf50* mRNA expression compared with diploid or deletion cases ($p = 4.95 \times 10^{-13}$; Fig. 3B). When stratified by FIGO stage, *C1orf50* expression showed a stepwise increase from stage II to stage IV disease, with a significant difference observed between stage II and stage IV tumors ($p = 0.027$; Fig. 3C). Together, these findings suggest that *C1orf50* amplification is a major contributor to its transcriptional upregulation, and may be linked to tumor progression and disease aggressiveness in ovarian cancer.

Proteomic profiling using RPPA identified multiple proteins whose abundance differed significantly between *C1orf50*-high and *C1orf50*-low tumors (Fig. 3D). The immune checkpoint molecule B7-H3 (*CD276*) showed the strongest upregulation in the high-expression group, alongside SGK3 and PRDX1, whereas phospho-PKCα (T638/T641), RHEB, and IGFBP3 were significantly reduced.

Unsupervised clustering of CIBERSORT-estimated immune cell fractions identified three characteristic immune clusters (C1-C3) (Fig. 3E). The C3 cluster, which had the highest *C1orf50* expression, was enriched in immunosuppressive cell types, including regulatory T cells (Tregs) and M2 macrophages. Collectively, these findings indicate that *C1orf50* amplification is associated with increased transcript expression and an immunosuppressive tumor microenvironment in ovarian cancer. To confirm the robustness of this immune clustering, we performed a bootstrap stability analysis (80% subsampling, B = 1000). The clustering structure was highly reproducible (median ARI = 0.889, interquartile range [IQR]: 0.757–0.941; median NMI = 0.832, IQR: 0.700–0.906), confirming the stability of the k = 3 solution.

Impact of *C1orf50* on cancer cell-immune cell communication networks

To explore how *C1orf50* expression influences cell–cell communication in the tumor immune microenvironment, we stratified cancer cells into *C1orf50*-high and *C1orf50*-low groups based on the median expression level using single-cell RNA-seq data from the ovarian cancer cohort [25]. Cell–cell communication networks were inferred using CellChat across 10 major cell types, including cancer cells, regulatory and effector T cells (Tregs), NK cells, macrophages, monocytes, and other immune populations. The UMAP plot showed the distribution of cell types used in the analysis, with cancer cells forming the majority, while immune cells were resolved (Fig. 4A). Comparison of intercellular communication revealed that the *C1orf50*-low group exhibited a greater number of ligand-receptor interactions (1,976) than the *C1orf50*-high group (1,626), along with slightly stronger overall interaction strength (57.2 vs. 56.4). These results suggest a modest attenuation of global cell–cell communication in tumors with elevated *C1orf50* expression (Fig. 4B). In the *C1orf50*-high group, cancer cells showed increased strength of cell–cell communication to all cell types, while non-cancer cells showed generally reduced signaling number and communication strength (Fig. 4C). We then explored the ligand-receptor pair connection between each cell type (Fig. 4D). In *C1orf50*-high cancer cells, we observed enhanced outgoing communication from cancer cells toward various immune subsets. Immunosuppressive interactions that include NECTIN2-TIGIT [26], MIF-(CD74 + CXCR4) [27, 28], PGE2-PTGER2 [29], and HLA-E-NKG2A [30] were upregulated in $CD4^+$ T cells, $CD8^+$ T cells, and NK cells, consistent with reduced anti-tumor immune activity. In addition, regulatory T cells (Tregs) received stronger signals through NECTIN2/3-TIGIT and LAMC2-CD44 [31], suggesting an enhanced immunosuppressive function of *C1orf50*. M1 and M2 macrophages showed increased engagement via LAM family-CD44 [31], MDK-NCL [32], APP-CD74 [33], and ICAM1-integrins [34], reflecting a tumor-supportive environment. B cells, DCs, and monocytes also received intensified adhesion- and growth-related signals such as ICAM1-integrins or MDK-NCL. Conversely, antigen presentation via HLA class II molecules from cancer cells to immune cells was reduced, along with attenuated signals to T/NK cells and macrophages via the CD99 axis [35], further supporting immune evasion in *C1orf50*-high tumors. To characterize how *C1orf50* expression influences immune microenvironment communication, we assessed pathway-level signaling from

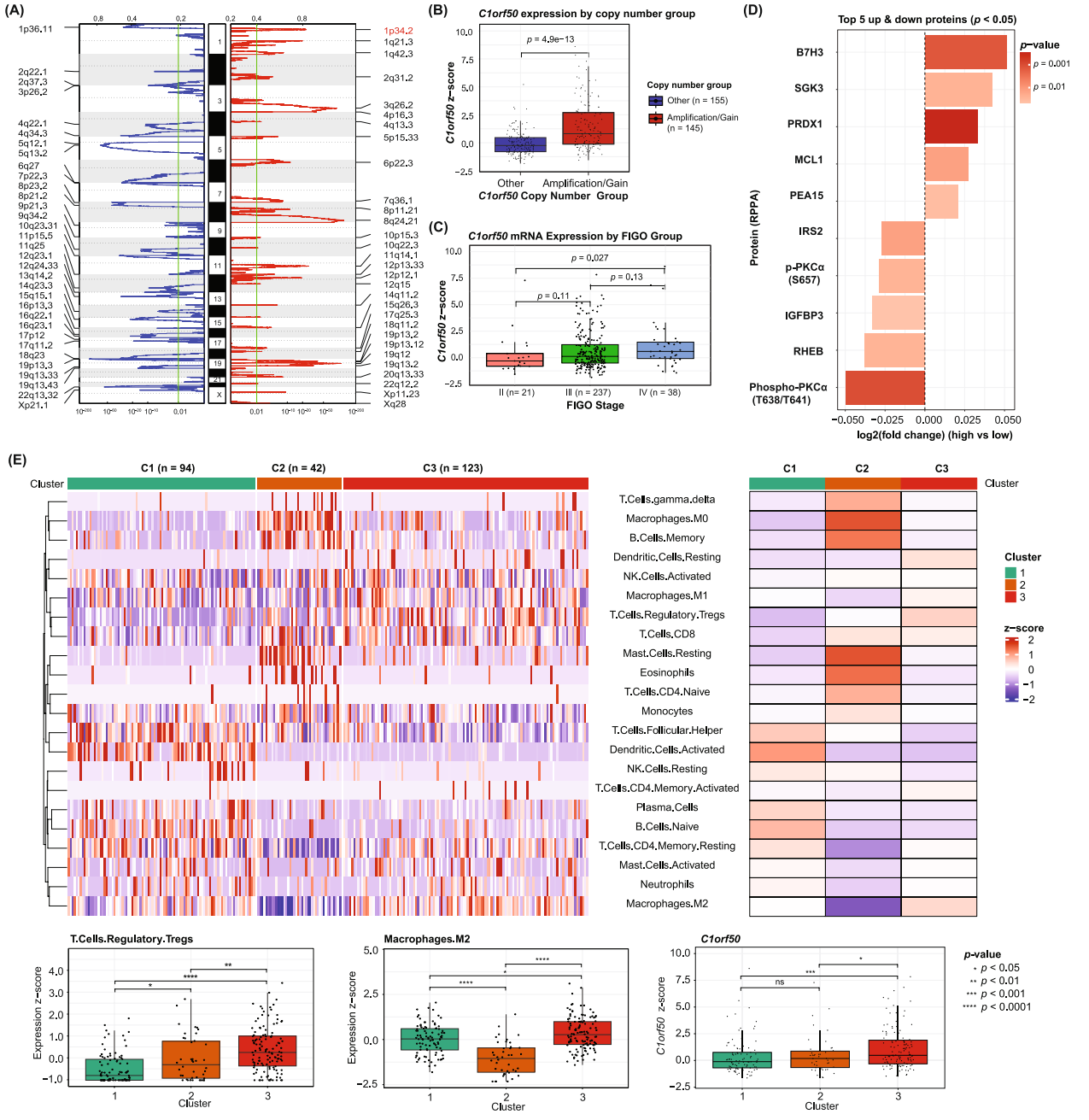

Fig. 3 *C1orf50* amplification is associated with increased expression and an immunosuppressive tumor microenvironment in ovarian cancer. **A** GISTIC2.0 analysis of the TCGA ovarian cancer cohort showing recurrent copy-number alterations across the genome. The 1p34.2 locus containing *C1orf50* is indicated. **B***C1orf50* mRNA expression stratified by copy-number status (Other = diploid or deletion; Amp/Gain = amplification or gain). **C***C1orf50* mRNA expression by FIGO stage (II, III, IV). **D** Top five significantly upregulated and downregulated proteins in *C1orf50*-high versus *C1orf50*-low tumors, identified by reverse-phase protein array (RPPA) analysis. Bars represent $\log_2$ fold change; p-values are indicated. **E** Unsupervised clustering of CIBERSORT-estimated immune cell fractions in ovarian cancer, identifying three immune clusters (C1-C3). Heatmaps show the immune cell composition (left) and the mean z-scores per cluster (right). Boxplots depict Treg and M2 macrophage abundance, and *C1orf50* mRNA expression, by cluster. Significance levels: * $p < 0.05$, ** $p < 0.01$, *** $p < 0.001$, **** $p < 0.0001$

cancer cells to immune subsets (Fig. 4E). *C1orf50*-high cancer cells showed elevated signaling toward CD8 + T cells through multiple pathways, including prostaglandin, APP, and LAMININ signaling. However, MIF signaling toward CD8 + T cells was reduced, potentially reflecting suppressed inflammatory cues. In relation to Treg and NK cells, *C1orf50*-high cancer cells exhibited elevated signaling through NECTIN, LAMININ, prostaglandin, MK (Midkine), and cholesterol-related pathways, all of which have been implicated in immune checkpoint

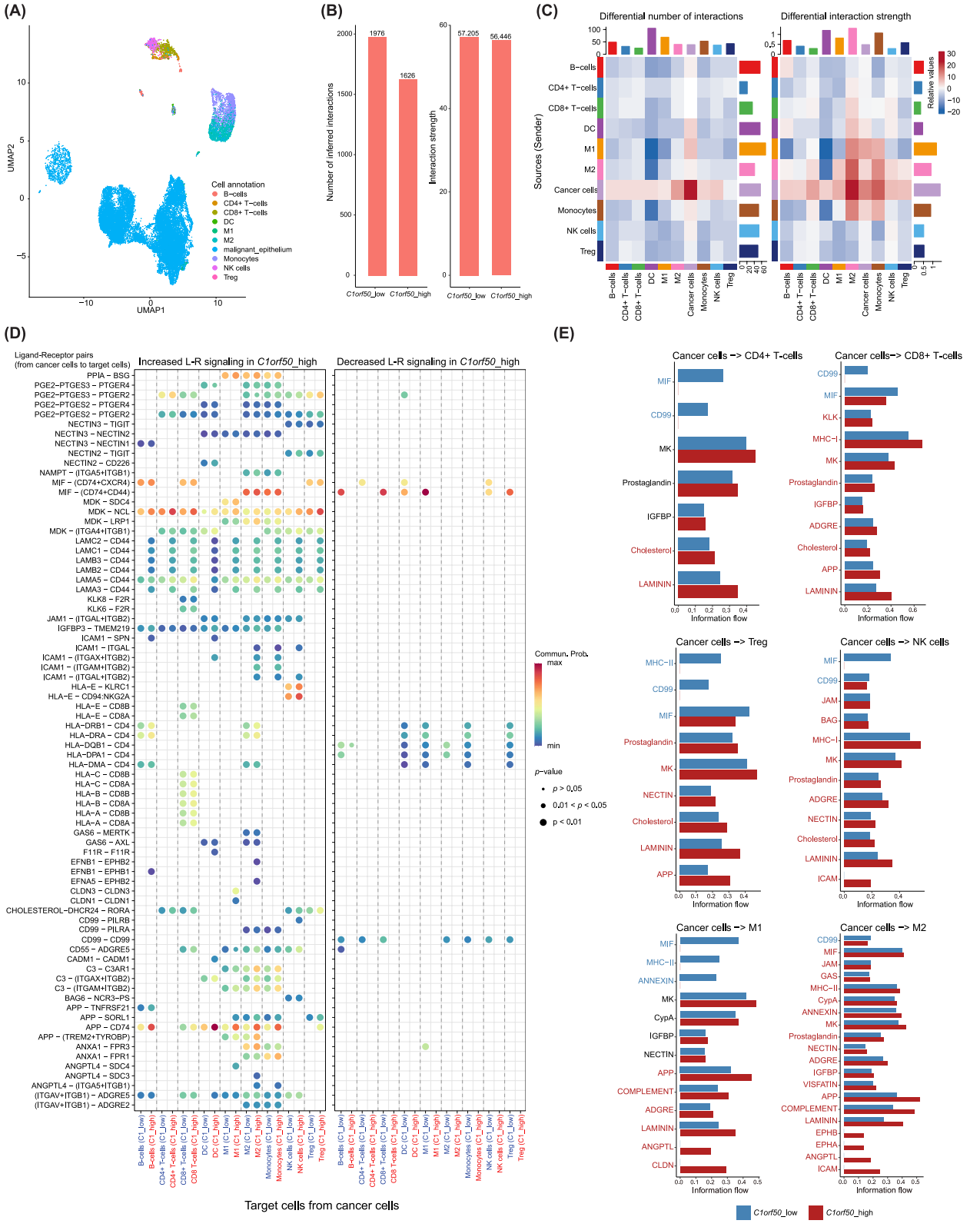

Fig. 4 (See legend on next page.)

(See figure on previous page.)

Fig. 4 *C1orf50*-associated modulation of tumor-immune cell communication networks in ovarian cancer single-cell transcriptomes. **A** UMAP plot of annotated cell types used for CellChat analysis. **B** Bar plots showing the total number of inferred ligand-receptor interactions and overall interaction strength in *C1orf50*-low and *C1orf50*-high groups. **C** Heatmaps depicting differences in the number (left) and strength (right) of interactions between source (y-axis) and receiver (x-axis) cell types. Red indicates higher signaling in the *C1orf50*-high group, blue indicates higher signaling in the *C1orf50*-low group. Top bar plots represent cumulative incoming signals, and side bar plots indicate outgoing signals. **D** Bubble plots of differentially enriched ligand-receptor pairs between *C1orf50*-high and *C1orf50*-low cancer cells. Dot size denotes statistical significance, and color indicates communication probability. Immune checkpoint- and suppression-related interactions (e.g., NECTIN-TIGIT, PGE2-PTGER, MIF-CD74) are enriched in *C1orf50*-high tumors. **E** Bar plots of pathway-level information flow from cancer cells to selected immune cell subsets, comparing *C1orf50*-high (red) and *C1orf50*-low (blue) tumors. Abbreviations: DC, dendritic cell; M1, M1 macrophage; M2, M2 macrophage. Information flow represents the overall communication strength of a signaling pathway

activity. The NECTIN-TIGIT axis was reinforced across Treg, NK, and M2 macrophage targets. For M1 and M2 macrophages, the *C1orf50*-high group showed increased communication through the LAMININ, APP, and complement pathways. At the same time, MHC class II signaling was reduced in M1 macrophages, indicating a shift toward a tolerogenic phenotype (fewer signals from M1 macrophages to T cells). These pathway-level changes suggest that *C1orf50*-high cancer cells create an immunosuppressive microenvironment by upregulating checkpoint and matrix-related pathways, while downregulating pro-inflammatory signals.

C1orf50 overexpression is associated with genomic instability and altered DNA repair pathway regulation in ovarian cancer

To evaluate the impact of *C1orf50* expression on DNA repair capacity in ovarian cancer, we compared genomic instability metrics, mutational signatures, and DNA repair gene expression between tumors with high and low *C1orf50* expression. As shown in Figs. 5A-C, *C1orf50*-high tumors exhibited significantly higher TMB ($p = 0.0044$), HRD scores ($p = 0.00031$), and LOH fractions ($p = 0.0037$) than the low-expression group. *BRCA1/2* gene alterations were also more frequent ($p = 0.012$), with a modest predominance of *BRCA2* events (Fig. 5D). Mutational signature analysis identified enrichment of single-base substitution signature 13 (SBS13) in *C1orf50*-high tumors (22.5% vs 9.7%, $p = 0.014$; Fig. 5E) and a greater prevalence of insertion-deletion signature 8 (ID8), which is linked to HRD (56.4% vs 44.6%, $p = 0.12$; Fig. 5F). Gene expression analysis (Fig. 5G) revealed a broad decrease in the expression of key DNA repair genes within the homologous recombination (HR), Fanconi anemia, and mismatch repair (MMR) pathways. This included genes such as *ATM, ATR, BARD1, BRCA1/2, FANCC, FANCD2, FANCI, MSH3, PMS2, PRKDC*, and *TP53BP1*. In contrast, several other repair-related genes, including *NHEJ1, PAXX, EPCAM, PCNA, RAD51B*, and *RAD51C*, showed significantly increased expression. In summary, *C1orf50* overexpression is strongly associated with extensive genomic instability in ovarian cancer, characterized by elevated TMB, HRD, LOH, distinct mutational and copy-number signatures, and extensive suppression of DNA repair pathways. The selective upregulation of specific repair components may reflect compensatory remodeling of the repair network supporting, tumor survival under high genomic stress.

Discussion

In this study, we conducted a comprehensive investigation of *C1orf50* using a pan-cancer cohort followed by an in-depth analysis focused on ovarian cancer. *C1orf50* overexpression is consistently associated with genomic instability and immune suppression, suggesting that this gene may be involved in pathways linking these two tumor hallmarks.

C1orf50 copy number gain and overexpression were detected across multiple tumor types, with the strongest signal observed in ovarian cancer (Figs. 1 and 2). Pan-cancer analysis revealed that high *C1orf50* expression was consistently associated with greater chromosomal instability and impaired DNA repair capacity, as evidenced by its positive correlation with TMB and HRD. *C1orf50*-high tumors also exhibited an immunosuppressive phenotype, characterized by the enrichment of regulatory T cells (Tregs) and the depletion of resting memory $CD4^+$ T cells, suggesting a role in promoting immune evasion.

Focusing on ovarian cancer (Figs. 3, 4, 5), we found that *C1orf50* amplification was a major contributor to its overexpression. *C1orf50*-high tumors displayed significantly elevated TMB, higher HRD scores, and increased frequencies of *BRCA1/2* alterations, consistent with defective homologous recombination repair. Pathway-level analysis revealed broad suppression of DNA repair processes, including the non-homologous end joining (NHEJ), the Fanconi anemia, and mismatch repair (MMR) pathways. At the same time, microsatellite instability-related gene sets were enriched in the high-expression group. At the gene level, most canonical repair genes (*ATM, ATR, BRCA1, BRCA2, FANCC, FANCD2, MSH3, PMS2*) were downregulated. In contrast, a subset of repair components (*NHEJ1, PAXX, EPCAM, PCNA, RAD51B, RAD51C*) was selectively upregulated, indicating a compensatory activation of alternative repair mechanisms that may help sustain tumor survival under genomic stress.

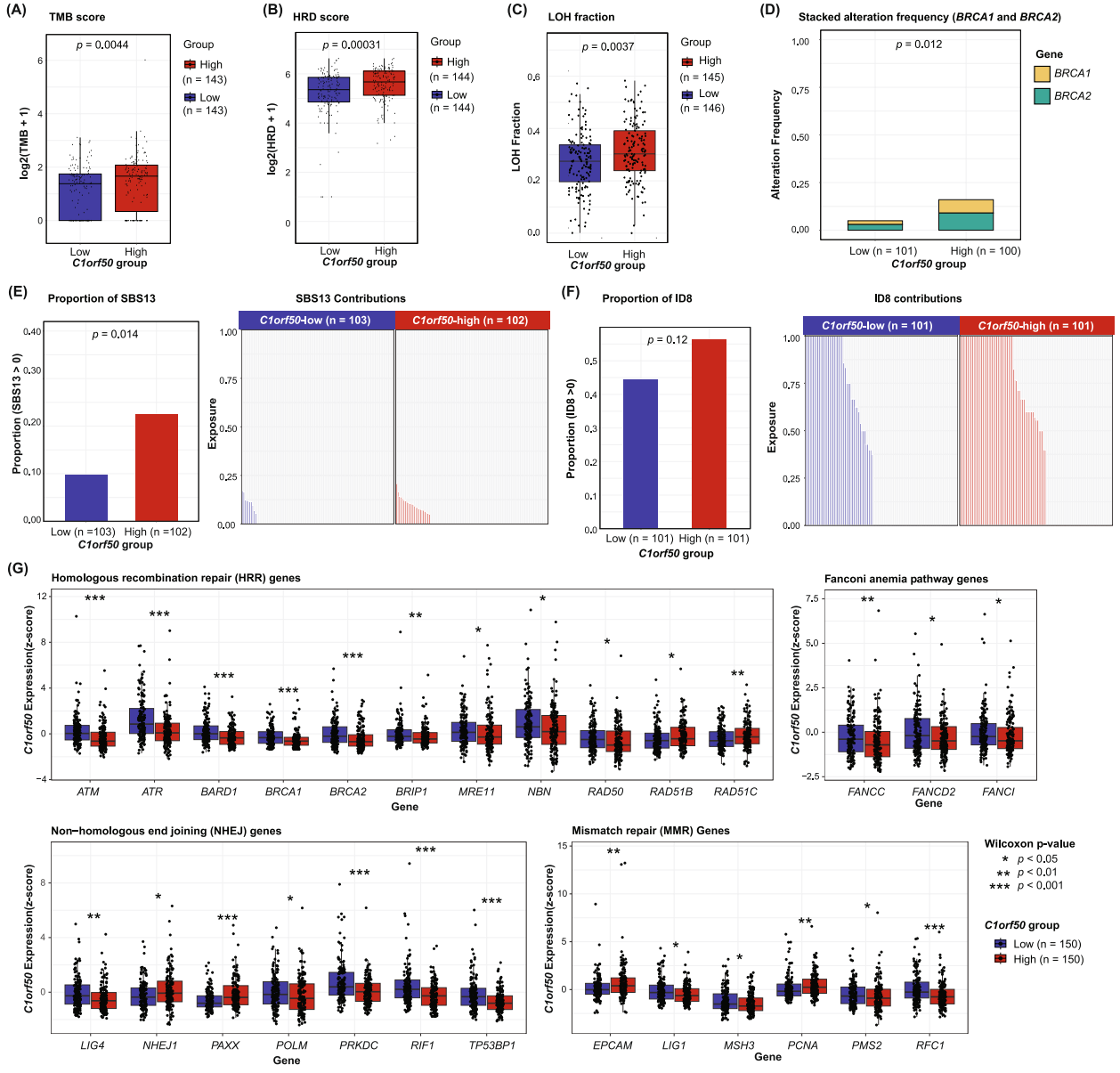

Fig. 5 *C1orf50* overexpression is associated with genomic instability and altered regulation of the DNA repair pathway in ovarian cancer. **A**-**C** Genomic instability metrics comparing *C1orf50*-high and *C1orf50*-low ovarian tumors, including tumor mutation burden (TMB; $p = 0.0044$), homologous recombination deficiency (HRD) scores ($p = 0.00031$), and loss of heterozygosity (LOH) fraction ($p = 0.0037$) (Wilcoxon rank-sum test). **D** Stacked alteration frequencies of *BRCA1* and *BRCA2*, showing a higher prevalence of *BRCA1/2* alterations in the *C1orf50*-high group ($p = 0.012$), with a modest predominance of *BRCA2* events (Fisher's exact test). **E**–**F** Mutational signature analysis demonstrating enrichment of the APOBEC-associated SBS13 (22.5% vs. 9.7%, $p = 0.014$; Fisher's exact test), and a higher prevalence of the HR-deficiency-associated ID8 (56.4% vs. 44.6%, $p = 0.12$; Fisher's exact test) in *C1orf50*-high tumors. **G** Expression of DNA repair genes across HRR, NHEJ, MMR, and Fanconi anemia pathways. Most core repair genes (*ATM, ATR, BARD1, BRCA1/2, FANCC/D2/I, MSH3, PMS2, PRKDC, TP53BP1*) were broadly downregulated, while a subset (*NHEJ1, PAXX, EPCAM, PCNA, RAD51B/C*) showed significant upregulation (Wilcoxon rank-sum test)

Proteomic profiling provided deeper insight into the molecular effects of *C1orf50* overexpression. RPPA analysis showed that *C1orf50*-high tumors had increased levels of the immune checkpoint molecule B7-H3 (*CD276*) and the antioxidant protein PRDX1, while displaying decreased phosphorylation of PKCα (T638/T641). The induction of B7-H3 aligns with the strong immunosuppressive signals observed at the transcriptomic and single-cell levels, supporting the idea that *C1orf50* may help tumors evade host immune responses. Upregulation of PRDX1 indicates these tumors are better able to neutralize reactive oxygen species [36, 37], which could give them a survival advantage under oxidative stress conditions common in the tumor environment. Conversely, the reduction in PKCα phosphorylation, often linked to adhesion and tumor-suppressive signaling [38, 39],

suggests a loss of regulation that may further promote tumor growth, invasion, and immune evasion. Overall, these proteomic changes demonstrate how *C1orf50* amplification coordinates both internal survival mechanisms and external immune-modulating processes, highlighting its potential as a therapeutic target in ovarian cancer.

Immune cell profiling confirmed that *C1orf50*-high ovarian tumors were enriched for Tregs and M2 macrophages, with elevated expression of immunosuppressive molecules. Cell–cell communication analysis revealed strengthened signaling through the NECTIN-TIGIT axis and other pathways supporting immune suppression and tumor tolerance. These features indicate that C1orf50 shapes a microenvironment that may hinder anti-tumor immunity and reduce responsiveness to immunotherapies.

In summary, these results highlight *C1orf50* as a potential oncogenic factor that promotes genomic instability while simultaneously fostering immune evasion in ovarian cancer. The combination of DNA repair defects and selective upregulation of alternative repair components suggests that *C1orf50*-high tumors may be particularly vulnerable to DNA-damaging agents, such as platinum compounds or PARP inhibitors. In parallel, the enrichment of immune checkpoint molecules, particularly B7-H3, together with increased infiltration of immunosuppressive cell types, suggests that these tumors may be amenable to immune checkpoint blockade, particularly in combination with DNA damage-targeted therapies. Such a dual approach could exploit both the impaired DNA repair machinery and the immunosuppressive signaling environment characteristic of these tumors. In addition, the observed downregulation of phosphorylated PKCα points to broader signaling alterations, as PKCα is involved in pathways regulating cell proliferation, survival, and immune modulation. Its reduced activity may therefore influence not only tumor cell-intrinsic behavior but also the dynamics of tumor-immune interactions, further shaping the therapeutic vulnerabilities of *C1orf50*-high tumors.

In conclusion, C1orf50 overexpression is strongly associated with genomic instability, DNA repair suppression, and an immunosuppressive tumor microenvironment in ovarian cancer. This study provides hypothesis-generating evidence that C1orf50 may serve as a molecular link between genomic instability and immune modulation, warranting further experimental validation.

Abbreviations

CIN	Chromosomal instability
CNA	Copy-number alteration
COSMIC	Catalogue of somatic mutations in cancer
EMT	Epithelial-mesenchymal transition
FGA	Fraction of genome altered
FIGO	International federation of gynecology and obstetrics
GEO	Gene expression omnibus
GSEA	Gene set enrichment analysis
HRD	Homologous recombination deficiency
HRR	Homologous recombination repair
LOH	Loss of heterozygosity
MMR	Mismatch repair
MSI	Microsatellite instability
MSigDB	Molecular signatures database
NES	Normalized enrichment score
NHEJ	Non-homologous end joining
PCA	Principal component analysis
RPPA	Reverse-phase protein array
SBS	Single base substitution (mutational signature)
scRNA-seq	Single-cell RNA sequencing
TCGA	The cancer genome Atlas
TCPA	The cancer proteome Atlas
TMB	Tumor mutational burden
TPM	Transcripts per million
Treg(s)	Regulatory T cell(s)
UMAP	Uniform manifold approximation and projection

Supplementary Information

The online version contains supplementary material available at https://doi.org/10.1186/s13048-025-01916-8.

Additional file 1. Supplemental figure 1.

Acknowledgements

We thank the TCGA Research Network (https://www.cancer.gov/tcga) for generating the genomic datasets and the cBioPortal for Cancer Genomics (https://www.cbioportal.org) for providing processed TCGA data. Single-cell RNA-seq data used in this study were obtained from the Gene Expression Omnibus (GEO) under accession number GSE158722.

Informed consent

Not applicable. The data used in this study were obtained from publicly available sources and do not contain any identifiable personal information.

Authors' contributions

A.R. and Y.O. contributed equally to this work: performed data analysis, visualization, original draft preparation, review, and editing. A.O., V.D.C., S.A.: performed data analysis, writing, review, and editing. T.P.: performed data analysis, visualization. S.T.: project administration, writing, review, and editing. A.F.: contributed to conceptualization, funding acquisition, investigation, supervision, writing of the original draft, review, and editing. A.T.: contributed to conceptualization, data curation, formal analysis, funding acquisition, investigation, methodology, project administration, resources, supervision, validation, writing of the original draft, review, and editing. All authors discussed the results and contributed to the final manuscript.

Data availability

We thank the TCGA Research Network (https://www.cancer.gov/tcga) for generating the genomic datasets and the cBioPortal for Cancer Genomics (https://www.cbioportal.org) for providing processed TCGA data. Single-cell RNA-seq data used in this study were obtained from the Gene Expression Omnibus (GEO) under accession number GSE158722.

Declarations

Ethical approval and consent to participate

This study used publicly available, de-identified data from The Cancer Genome Atlas (TCGA) and previously published studies. Therefore, Institutional Review Board (IRB) approval and informed consent were not required.

Consent for publication

Not applicable.

Competing interests

The authors declare no competing interests.

Author details
[1]Department of Pathology, Beth Israel Deaconess Medical Center, Harvard Medical School, 330 Brookline Avenue, Boston, MA 02115, USA
[2]Harvard Medical School, Boston, MA, USA
[3]Department of Medicine and Cancer Center, Beth Israel Deaconess Medical Center, Boston, MA 02115, USA
[4]Department of Urology, Gunma University Graduate School of Medicine, 3-9-22 Showa-Machi, Maebashi, Gunma 371-8511, Japan
[5]UMass Chan Medical School, UMass Memorial Medical Center, 55 Lake Ave. North, Worcester, MA 01655, USA
[6]Department of General Thoracic Surgery and Breast and Endocrinological Surgery, Dentistry and Pharmaceutical Sciences, Okayama University Graduate School of Medicine, Kita-Ku, Okayama 700-8558, Japan
[7]Department of Molecular Physiology, Faculty of Medicine, Graduate School of Medicine, Kagawa University, 1750-1 Ikenobe, Miki-Cho, Kita-Gun, Kagawa 761-0793, Japan
[8]Broad Institute of MIT and Harvard, Cambridge, MA, USA

Received: 3 September 2025 / Accepted: 23 November 2025
Published online: 08 December 2025

References

1. Jumper J, Evans R, Pritzel A, Green T, Figurnov M, Ronneberger O, et al. Highly accurate protein structure prediction with AlphaFold. Nature. 2021;596(7873):583–9.
2. Otani Y, Maekawa M, Tanaka A, Peña T, Chin VD, Rogachevskaya A, et al. C1orf50 drives malignant melanoma progression through the regulation of stemness. Cancer Genomics Proteomics. 2025;22(4):510–24.
3. Tanaka A, Otani Y, Maekawa M, Rogachevskaya A, Peña T, Chin VD, et al. C1orf50 accelerates epithelial-mesenchymal transition and the cell cycle of hepatocellular carcinoma. Cancer Genomics Proteomics. 2025;22(6):836–49.
4. Otani Y, Tanaka A, Maekawa M, Peña T, Rogachevskaya A, Ando T, et al. The role of C1orf50 in breast cancer progression and prognosis. Breast Cancer. 2025;32(2):292–305.
5. Davis SJ, Sheppard KE, Pearson RB, Campbell IG, Gorringe KL, Simpson KJ. Functional analysis of genes in regions commonly amplified in high-grade serous and endometrioid ovarian cancer. Clin Cancer Res. 2013;19(6):1411–21.
6. Henderson LJ, Coe BP, Lee EH, Girard L, Gazdar AF, Minna JD, et al. Genomic and gene expression profiling of minute alterations of chromosome arm 1p in small-cell lung carcinoma cells. Br J Cancer. 2005;92(8):1553–60.
7. Fix A, Peter M, Pierron G, Aurias A, Delattre O, Janoueix-Lerosey I. High-resolution mapping of amplicons of the short arm of chromosome 1 in two neuroblastoma tumors by microarray-based comparative genomic hybridization. Genes Chromosomes Cancer. 2004;40(3):266–70.
8. Beroukhim R, Mermel CH, Porter D, Wei G, Raychaudhuri S, Donovan J, et al. The landscape of somatic copy-number alteration across human cancers. Nature. 2010;463(7283):899–905.
9. Zack TI, Schumacher SE, Carter SL, Cherniack AD, Saksena G, Tabak B, et al. Pan-cancer patterns of somatic copy number alteration. Nat Genet. 2013;45(10):1134–40.
10. McGranahan N, Furness AJ, Rosenthal R, Ramskov S, Lyngaa R, Saini SK, et al. Clonal neoantigens elicit T cell immunoreactivity and sensitivity to immune checkpoint blockade. Science. 2016;351(6280):1463–9.
11. Team RC. R: A language and environment for statistical computing Vienna, Austria: R Foundation for Statistical Computing; 2025. Available from: https://www.R-project.org/.
12. Cerami E, Gao J, Dogrusoz U, Gross BE, Sumer SO, Aksoy BA, et al. The cBio cancer genomics portal: an open platform for exploring multidimensional cancer genomics data. Cancer Discov. 2012;2(5):401–4.
13. Gao J, Aksoy BA, Dogrusoz U, Dresdner G, Gross B, Sumer SO, et al. Integrative analysis of complex cancer genomics and clinical profiles using the cBioPortal. Sci Signal. 2013;6(269):pl1.
14. Thorsson V, Gibbs DL, Brown SD, Wolf D, Bortone DS, Ou Yang TH, et al. The Immune Landscape of Cancer. Immunity. 2018;48(4):812-30.e14.
15. Taylor AM, Shih J, Ha G, Gao GF, Zhang X, Berger AC, et al. Genomic and functional approaches to understanding cancer aneuploidy. Cancer Cell. 2018;33(4):676-89.e3.
16. Zhao Y, Li MC, Konaté MM, Chen L, Das B, Karlovich C, et al. TPM, FPKM, or normalized counts? A comparative study of quantification measures for the analysis of RNA-seq data from the NCI patient-derived models repository. J Transl Med. 2021;19(1):269.
17. Hoadley KA, Yau C, Hinoue T, Wolf DM, Lazar AJ, Drill E, et al. Cell-of-origin patterns dominate the molecular classification of 10,000 tumors from 33 types of cancer. Cell. 2018;173(2):291-304.e6.
18. Hao Y, Stuart T, Kowalski MH, Choudhary S, Hoffman P, Hartman A, et al. Dictionary learning for integrative, multimodal and scalable single-cell analysis. Nat Biotechnol. 2024;42(2):293–304.
19. Korsunsky I, Millard N, Fan J, Slowikowski K, Zhang F, Wei K, et al. Fast, sensitive and accurate integration of single-cell data with harmony. Nat Methods. 2019;16(12):1289–96.
20. Li J, Lu Y, Akbani R, Ju Z, Roebuck PL, Liu W, et al. TCPA: a resource for cancer functional proteomics data. Nat Methods. 2013;10(11):1046–7.
21. Li J, Akbani R, Zhao W, Lu Y, Weinstein JN, Mills GB, et al. Explore, visualize, and analyze functional cancer proteomic data using the Cancer Proteome Atlas. Cancer Res. 2017;77(21):e51–4.
22 Uhlén M, Fagerberg L, Hallström BM, Lindskog C, Oksvold P, Mardinoglu A, et al. Proteomics. Tissue-based map of the human proteome. Science. 2015;347(6220):1260419.
23. Gu Z, Eils R, Schlesner M. Complex heatmaps reveal patterns and correlations in multidimensional genomic data. Bioinformatics. 2016;32(18):2847–9.
24. Jin S, Guerrero-Juarez CF, Zhang L, Chang I, Ramos R, Kuan CH, et al. Inference and analysis of cell-cell communication using cell chat. Nat Commun. 2021;12(1):1088.
25. Nath A, Cosgrove PA, Mirsafian H, Christie EL, Pflieger L, Copeland B, et al. Evolution of core archetypal phenotypes in progressive high grade serous ovarian cancer. Nat Commun. 2021;12(1):3039.
26. Chauvin JM, Zarour HM. TIGIT in cancer immunotherapy. J Immunother Cancer. 2020;8(2):e000957.
27. Farr L, Ghosh S, Moonah S. Role of MIF Cytokine/CD74 receptor pathway in protecting against injury and promoting repair. Front Immunol. 2020;11:1273.
28. Gore Y, Starlets D, Maharshak N, Becker-Herman S, Kaneyuki U, Leng L, et al. Macrophage migration inhibitory factor induces B cell survival by activation of a CD74-CD44 receptor complex. J Biol Chem. 2008;283(5):2784–92.
29. Francica BJ, Holtz A, Lopez J, Freund D, Chen A, Wang D, et al. Dual blockade of EP2 and EP4 signaling is required for optimal immune activation and antitumor activity against prostaglandin-expressing tumors. Cancer Res Commun. 2023;3(8):1486–500.
30. Sætersmoen M, Kotchetkov IS, Torralba-Raga L, Mansilla-Soto J, Sohlberg E, Krokeide SZ, et al. Targeting HLA-E-overexpressing cancers with a NKG2A/C switch receptor. Med. 2025;6(2):100521.
31. Erice O, Narayanan S, Feliu I, Entrialgo-Cadierno R, Malinova A, Vicentini C, et al. LAMC2 regulates key transcriptional and targetable effectors to support pancreatic cancer growth. Clin Cancer Res. 2023;29(6):1137–54.
32. Fu Y, Li S, Zhao Y, Zhang X, Mao X, Xu R. Integrative single-cell and spatial transcriptomics analysis reveals MDK-NCL pathway's role in shaping the immunosuppressive environment of lung adenocarcinoma. Front Immunol. 2025;16:1546382.
33. Chen G, Wang W, Wei X, Chen Y, Peng L, Qu R, et al. Single-cell transcriptomic analysis reveals that the APP-CD74 axis promotes immunosuppression and progression of testicular tumors. J Pathol. 2024;264(3):250–69.
34. Chen M, Wu C, Fu Z, Liu S. ICAM1 promotes bone metastasis via integrin-mediated TGF-β/EMT signaling in triple-negative breast cancer. Cancer Sci. 2022;113(11):3751–65.
35. Mannion AJ, Odell AF, Taylor A, Jones PF, Cook GP. Tumour cell CD99 regulates transendothelial migration via CDC42 and actin remodelling. J Cell Sci. 2021;134(15):jcs240135.
36. Ding C, Fan X, Wu G. Peroxiredoxin 1 - an antioxidant enzyme in cancer. J Cell Mol Med. 2017;21(1):193–202.
37. Hampton MB, Vick KA, Skoko JJ, Neumann CA. Peroxiredoxin involvement in the initiation and progression of human cancer. Antioxid Redox Signal. 2018;28(7):591–608.
38. Newton AC, Brognard J. Reversing the paradigm: protein kinase C as a tumor suppressor. Trends Pharmacol Sci. 2017;38(5):438–47.
39. Oster H, Leitges M. Protein kinase C alpha but not PKCzeta suppresses intestinal tumor formation in ApcMin/+ mice. Cancer Res. 2006;66(14):6955–63.

Publisher's Note